Complete Modal Decomposition for Optical Waveguides

Ofer Shapira,[1] Ayman F. Abouraddy,[1] John D. Joannopoulos,[1,2] and Yoel Fink[1,2,*]

[1]*Research Laboratory of Electronics, Massachusetts Institute of Technology, Cambridge, Massachusetts 02139, USA*
[2]*Center for Materials Science and Engineering, Massachusetts Institute of Technology, Cambridge, Massachusetts 02139, USA*

(Received 10 December 2004; published 14 April 2005)

Virtually all electromagnetic waveguiding structures support a multiplicity of modes. Nevertheless, to date, an experimental method for unique decomposition of the fields in terms of the component eigenmodes has not been realized. The fundamental problem is that all current attempts of modal decomposition do not yield phase information. Here we introduce a noninterferometric approach to achieve modal decomposition of the fields at the output of a general waveguiding structure. The technique utilizes a mapping of the two-dimensional field distribution onto the one-dimensional space of waveguide eigenmodes, together with a phase-retrieval algorithm to extract the amplitudes and phases of all the guided vectorial modes. Experimental validation is provided by using this approach to examine the interactions of 16 modes in a hollow-core photonic-band gap fiber.

DOI: 10.1103/PhysRevLett.94.143902 PACS numbers: 42.25.Bs, 42.30.Rx, 42.70.Qs, 42.81.Qb

Eigenmode decomposition of the field at the output of waveguides can provide fundamental insights into the nature of electromagnetic-wave propagation. The comparison of the modes present at the input to those exiting the structure enables the elucidation of loss mechanisms on the one hand and quantitative analysis of modal coupling on the other. The prospect of performing modal decomposition is of importance to several recent experimental efforts in atom guiding [1], high-harmonic generation in atomic gases [2], supercontinuum generation [3], and core vs surface mode guidance in photonic-band gap (PBG) fibers [4]. Nevertheless, a practical route to comprehensive modal decomposition, one that yields the full complex expansion coefficients of the vectorial field in the eigenmode basis, has not yet been achieved. In this Letter we introduce a novel, rapidly converging, method based on the phase-retrieval algorithm together with intensity measurements at two planes, that yields a unique modal decomposition. An experimental validation is performed by decomposing the guided field in a photonic-band gap fiber. Both the amplitudes and phases of the 16 lowest-energy vectorial modes are obtained. The efficient convergence enables, for the first time, the quantitative analysis of bend-induced interactions in a many-mode system.

Indeed, research on the transmission properties of waveguides supporting a multiplicity of modes spans many decades, from millimeter waves in the seminal work of Southworth in the 1930s [5] through ultraviolet transmission [6] in recent experiments. Modal decomposition approaches based on single-intensity measurements in the Fourier plane have been known (Refs. [7,8], for example). However, without any other *a priori* known constraint of the field distribution, the solution of such an inverse problem is not unique [9–12]. An example for such ambiguity is demonstrated in Fig. 1 where we plot the measured intensity at the output of an optical fiber. Two possible amplitude decompositions (amongst many other) are provided, both of which yield a reconstruction that fits the measured intensity distribution.

Our approach is based on indirectly accessing the phase of the optical wave front at the output of the waveguide from intensity measurements alone. The Gerchberg-Saxton (GS) algorithm [10] is a particularly successful method for phase retrieval that results in a unique as well as noise tolerant solution [11] by iterating back and forth between the two-dimensional (2D) field distributions of the object and the Fourier planes (and thus can be quite computationally intensive). The decomposition of a field in a waveguide, on the other hand, is inherently a *one-dimensional* (1D) problem since the field is constrained to be a linear superposition of the waveguide eigenmodes that can be determined from the waveguide structure. The only unknowns are thus the expansion coefficients in this superposition, which form a 1D complex space. By mapping the problem from the 2D image space into this abstract 1D space of waveguide eigenmodes we reduce significantly the number of independent variables, and also completely remove the dependency on the number of pixels in the iterative process. Furthermore, since higher-order modes in

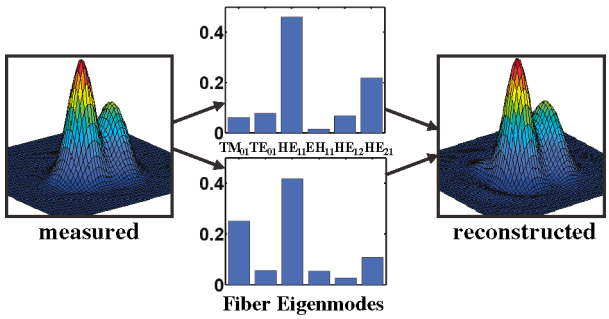

FIG. 1 (color). Two *distinct* amplitude decompositions, in the waveguide eigenmode basis, for a far-field intensity measured at the waveguide output. Both yield a reconstruction that fits the measured intensity.

multimode waveguides tend to have higher losses, one can set a modal cutoff, depending on the specifics of the waveguide, and deal with only a finite number of modes. It is noteworthy that this approach applies to *any* waveguide, whether or not it possesses any symmetry.

In Ref. [12], Fienup established that iterative methods, such as the GS algorithm, are related to gradient search methods. Following suit, we construct our algorithm to minimize an error function with respect to a set of independent variables representing the expansion coefficients of a basis set constructed of the waveguide eigenmodes. Since the vectorial aspect of the waveguide modes is essential we define four squared-error functions for two orthogonally polarized components in both the near and far fields

$$\Delta_{a,b} = \int_{\text{core}} \{I_{\text{r}}^{a,b}(\mathbf{r}) - I_{\text{me}}^{a,b}(\mathbf{r})\}^2 dA, \tag{1}$$

where $a = 1, 2$ defines the plane of measurement (near or far field), $b = 1, 2$ defines one of two perpendicular polarizations, I_{me} is the *measured* intensity, while I_{r} is the intensity of a *reconstructed* estimate of this field. We then define an overall error function $\Delta = \Sigma_{a,b}\Delta_{a,b}$. We used an unconstrained optimization routine [13] to perform the minimization of this error function over the space of expansion coefficients.

If the electric and magnetic field vectors of the nth waveguide mode are $\vec{\varphi}_n^{(E)}$ and $\vec{\varphi}_n^{(H)}$, respectively, and their scalar projections in a fixed direction are e_n and h_n, then the total field vectors are $\vec{E}(\mathbf{r}) = \Sigma_n c_n \vec{\varphi}_n^{(E)}(\mathbf{r})$, $\vec{H}(\mathbf{r}) = \Sigma_n c_n \vec{\varphi}_n^{(H)}(\mathbf{r})$, where $c_n = |c_n| e^{i\psi_n}$ are the expansion coefficients. Using this notation, the reconstructed intensity is $I_{\text{r}}(\mathbf{r}) = \frac{1}{N} \text{Re}\Sigma_{i,j} c_i c_j^* e_i(\mathbf{r}) h_j(\mathbf{r})$, where N is a normalization factor, and we note that e_i and h_j may be chosen to be real functions in two-dimensional structures. By rearranging, we may write any of the four error functions $\Delta_{a,b}$ as follows

$$\frac{1}{N^2} \sum_{ijpq} c_i c_j c_p^* c_q^* \Lambda_{ijpq} - \frac{2}{N} \sum_{ij} c_i c_j^* \Gamma_{ij} + P \tag{2}$$

where P is the integral over space of I_{me} squared, $\Lambda_{ijpq} = \int e_i(\mathbf{r}) e_j(\mathbf{r}) h_p(\mathbf{r}) h_q(\mathbf{r}) dA$, and $\Gamma_{ij} = \int I_{\text{me}}(\mathbf{r}) e_i(\mathbf{r}) h_j(\mathbf{r}) dA$. The tensors Λ and Γ may be contracted significantly by exploiting the symmetry of the waveguide modes. Furthermore, the tensor elements are computed once prior to the optimization of Δ, leading to a pixel-invariant iterative process.

For the sake of demonstrating a concrete application of our algorithm, we restrict ourselves for the remainder of the Letter to circularly symmetric waveguides. The cylindrical structure results in three conserved quantities that characterize the vectorial eigenmodes: the frequency ω, the axial-wave vector (eigenvalue) k, and the angular momentum m. The components of an eigenfunction with eigenvalue k has the form $R_{ml}(r)\cos(m\theta + \phi) \times \exp[i(kz - \omega t)]$. The phase ϕ, which we henceforth call the degeneracy phase, is required by the degeneracy of the $\sin m\theta$ and $\cos m\theta$ solutions of the wave equation. Modes with $m = 0$ are nondegenerate TE and TM, while modes with nonzero m are doubly degenerate hybrid modes [14,15]. The radial factor, $R_{ml}(r)$, can be obtained using the transfer-matrix method [16].

We confirmed the validity of this algorithm by applying it to the problem of mode decomposition in a multimode cylindrical photonic-band gap fiber [16,17]. The fiber [Fig. 2(a)] has a 533 μm-diameter hollow core surrounded by a multilayer structure that results in a fundamental band gap ranging from 9.5 to 11.2 μm. Since the core diameter is approximately 50 wavelengths, the fiber is highly multimoded and can in theory support about 2000 guided modes. In practice, however, the strong mode-filtering mechanism characteristic of this fiber [18], as well as the input coupling, result in only a few low-loss, low-energy modes remaining with considerable power after 1 m of fiber. We used a linearly polarized CO_2 laser at 10.6 μm to excite the fiber, and carried out three sets of measurements that we refer to as the long-fiber, bent-fiber, and short-fiber cases. In the long-fiber case, we carried out measurements for a 1.5 m long straight fiber; in the bent-fiber case, the first 1.1 m of the same fiber was kept straight while the rest is bent (radius of curvature $R_b = 0.3$ m, length $d = 0.4$ m); and in the short-fiber case, the bent part was cut off, leaving a 1.1 m long straight fiber. In each case we captured the near-field and far-field intensity images (using $4 - f$ and $2 - f$ lens configurations, respectively) of two orthogonal polarizations with a Spiricon pyroelectric camera preceded with a linear polarizer.

We performed the decompositions using a basis consisting of the 16 lowest-energy modes with angular momentum $m < 4$. We checked convergence by increasing the number of eigenfunctions in the chosen basis to incorpo-

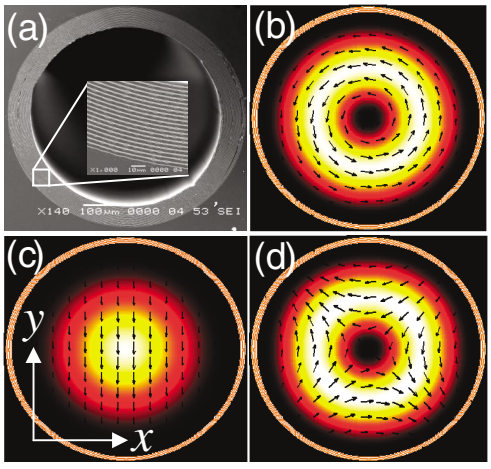

FIG. 2 (color). (a) Scanning electron microscope image of the PBG fiber cross section. Calculated intensities and vector field distributions for the (b) TE_{01}, (c) HE_{11}, and (d) HE_{21}. All plotted with the degeneracy phases ϕ_n set to 0.

rate higher-order modes and found no measurable improvement. The fidelity of the decomposition results to the measured intensity distributions is demonstrated in Fig. 3, for the short-fiber case. To further confirm the validity of this decomposition, all measurements were repeated for five distinct pairs of orthogonal polarization directions, and the correlation coefficients between the decomposition results exceeded 0.98. To verify convergence of the error function to its global minimum, we repeated the process for 50 different random initial conditions, and the correlation between the results was greater then 0.999.

Numerous salient features of wave propagation in the fiber may be discerned from the decomposition results of the three cases by virtue of unveiling the values for the amplitudes $|c_n|$, relative phases ψ_n, and degeneracy phases ϕ_n of the guided modes. We note that phase values are not reliable for modes with negligible amplitudes. We start by examining the short-fiber case [Fig. 4(a)], in which HE_{11} is the dominant mode [due to the strong overlap between the laser Gaussian-beam profile and the HE_{11} profile as shown in Fig. 2(c)], with contributions from other modes, most significantly TE_{01} and HE_{21}. The polarization of the output field was found to conserve the horizontal (x) polarization of the input field, as expected by the circular symmetric structure. Inspection of the values of $|c_n|$, ψ_n, and ϕ_n for the three above mentioned dominant modes confirms this experimental observation. This can be shown by first noting that in a large-core fiber the degeneracy phase ϕ_n of any mode manifests itself as a rotation of the mode field lines by an angle ϕ_n. In the case of HE_{11}, $\phi_{HE_{11}} \simeq \pi/2$ [upper panel of Fig. 4(a)], corresponding to a rotation of the field lines [Fig. 2(c)] to the horizontal. The TE_{01} and HE_{21} modes [Figs. 2(b) and 2(d)], on the other hand, have y-polarized components, but it is straightforward to show that the relative amplitude, phase, and degeneracy phase revealed by the decomposition ensure their cancellation.

In a straight fiber, the orthogonal modes propagate with no mutual interaction, thus, any changes in the modal distribution along its length are due to losses and dispersion. The amplitude of a mode in the output of the long fiber is related to that of the same mode in the short fiber by a factor of $e^{(ik_n-\alpha_n)d}$. Moreover, in the absence of structural perturbations we expect the degeneracy phases ϕ_n to retain their values. We theoretically calculated the axial-wave vectors k_n and loss coefficients α_n for our structure using the leaky-mode technique [19]. Figure 4(b) depicts a comparison between two modal decompositions for the long fiber for modes with $|c|^2 > 0.05$. The first is obtained directly from measurements performed on the long fiber, while the second uses the experimentally determined decomposition of the short fiber as initial condition for numerically evaluating the decomposition of the long fiber. The good agreement between the two cases is easily observed, and the correlation for both the amplitudes and degeneracy phases was found to be greater then 0.95. We attribute the small variations in the results to deviation of

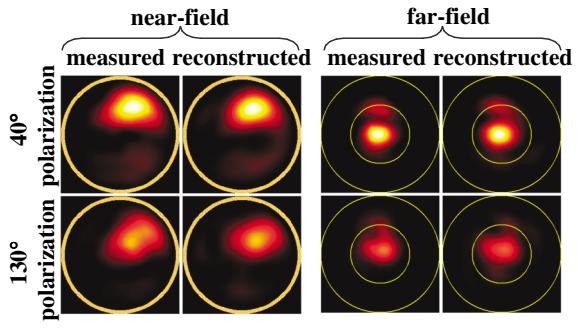

FIG. 3 (color). Measured and reconstructed intensity distributions for the short-fiber case. The circle in the near-field images represents the location of the fiber core-cladding interface. The two circles in the far-field images represent the location of the first and second zeros of a far-field image of a uniformly distributed field having the shape and extent of the fiber core.

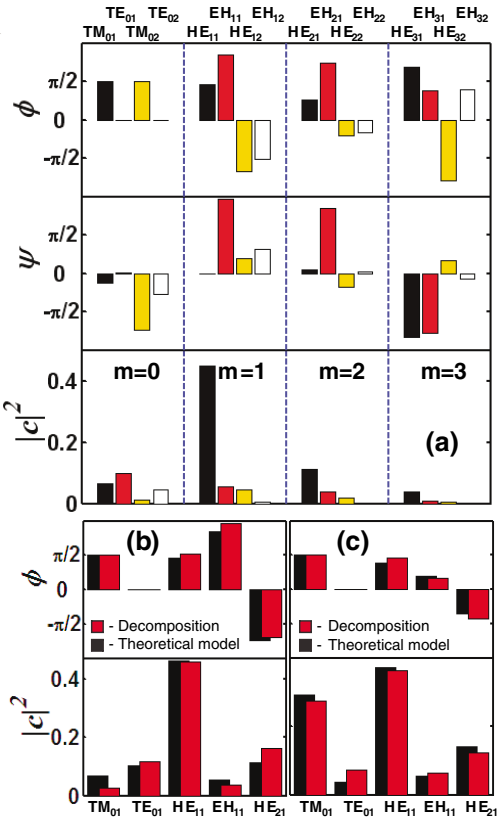

FIG. 4 (color). (a) Complete modal decomposition of the 16 lowest-energy modes, with angular momentum $m \leq 4$ for the short-fiber case. The lower, middle, and upper panels depict the expansion coefficients modulus squared $|c_n|^2$ (normalized such that $\sum |c_n|^2 = 1$), the relative phases ψ_n, and the degeneracy phases ϕ_n, respectively. (b) The decomposition results of the long fiber (red bars) and a theoretical estimation (black bars). (c) The decomposition results of the bent fiber (red bars) and the calculated results based on a mode-coupling model (black bars). Both theoretical estimates shown in (b) and (c) use the results in (a) as initial conditions.

the fiber structure [17] from the ideal cylindrical structure assumed by our theoretical model. While the amplitudes and degeneracy phases are quite insensitive to such structural deviations, accurate theoretical determination of the rapidly varying phases ψ_n require precise knowledge of both the wave vectors k_n and the absolute fiber length. A detailed experimental study on relative-phase reconstruction will be presented elsewhere.

The rapid convergence of our scheme and complete phase and amplitude information allows for the study of systems with a large number of interacting modes as is the case in a waveguide bend. Here we compare the modal content in a bent fiber obtained by direct experimental observation and subsequent modal decomposition at the fiber output to the predicted output based on coupled-mode theory assuming identical initial conditions established by the modal decomposition of a short fiber. Theoretically, bends with unchanged cross section and radius R_b much larger then the core radius, are treated as a perturbation to the fiber axis [18]. The field at the output of the bent fiber can then be represented by a linear superposition of the unperturbed fiber eigenmodes, with the coefficients satisfying

$$\frac{dc_n}{dz} = ik_n c_n + i\sum_{n' \neq n} \gamma_{nn'} c_{n'}, \tag{3}$$

where the matrix elements $\gamma_{nn'}$ representing the coupling between the n and n' modes and couples directly only those pairs of modes with $\Delta m = \pm 1$ [20], due to the nature of the perturbation. The degeneracy of modes with $m > 0$ is lifted under this perturbation, giving rise to a change in the degeneracy phases. Furthermore, the first nonzero correction to the coefficients in perturbation theory is inversely proportional to $\Delta k_{nn'} \equiv k_n - k_{n'}$, thus we expect only those modes that are close in k space to be strongly coupled. Evaluation of k_n for the various modes identifies TM_{01}, TE_{01}, and HE_{21} as the closest neighbors of HE_{11}. However, since the fiber bend was in the $x - z$ plane, reflection symmetry around the y axis must be conserved. Consequently, the x-polarized HE_{11} will not couple to TE_{01} due to their different symmetry under reflection in the y axis (Fig. 2). We solve Eq. (3) numerically for the modes shown in Fig. 4(c), taking the decomposition results for the short-fiber case as initial conditions. Figure 4(c) depicts the solution of the coupled-mode equations thus obtained alongside the decomposition results for the bent-fiber case and good agreement is observed with correlation coefficients for both amplitudes and degeneracy phases greater then 0.96. The expected coupling to TM_{01} is clear, while the ostensibly weaker coupling to HE_{21} can be understood from examining the dependence of the solution of Eq. (3) on the length of the bend. The modes exchange power back and forth along the bend due to interference of the scattered waves, and the length of the bend in our experiment fortuitously corresponds to a point at which the HE_{21} coefficient returns to its initial value. Lastly we note that if the polarization of the field lies in the plane of the fiber bend, the mode-coupling results in a field that conserves the original polarization, otherwise energy is transferred to the orthogonal polarization. For that reason the HE_{11} mode retains its polarization along x, as indicated by $\phi_{HE_{11}}$ (upper panel of Fig. 4(c)]. On the other hand, the degeneracy phase for the HE_{21} mode, which has both x-polarization and y-polarization components [see Fig. 2(d)] changes in order to maintain the overall x polarization while accommodating changes in the amplitudes of the other modes. The modal content as obtained by the two independent approaches is in close agreement as evident in Fig. 4(c).

In conclusion, we have presented an approach to perform complete modal decomposition for fields in optical waveguides. This noninterferometric approach is a modified phase-retrieval algorithm that makes use of the constraints placed on the field by the waveguide. This approach is applicable to any waveguide geometry and needs only knowledge of its eigenmodes. We demonstrated this technique by applying it to the optical field in a hollow-core photonic-band gap fiber and presented excellent agreement between the measured results and theoretical models.

This work was supported in part by DARPA, the ARO, the ONR, the AFOSR HEL-MURI, the US DOE, the ISN, and the Materials Research Science and Engineering Center (MRSEC) programme of the NSF.

*URL: http://mit-pbg.mit.edu/
Electronic address: yoel@mit.edu

[1] M. J. Renn *et al.*, Phys. Rev. Lett. **75**, 3253 (1995).
[2] E. Constant *et al.*, Phys. Rev. Lett. **82**, 1668 (1999).
[3] J. H. V. Price *et al.*, Appl. Phys. B **77**, 291 (2003).
[4] C. M. Smith *et al.*, Nature (London) **424**, 657 (2003).
[5] G. C. Southworth, Bell Syst. Tech. J. **15**, 284 (1936).
[6] Y. Matsuura *et al.*, Opt. Express **6**, 257 (2000).
[7] M. Skorobogatiy *et al.*, Opt. Express **11**, 2838 (2003).
[8] Y. Matsuura *et al.*, Electron. Lett. **30**, 1688 (1994).
[9] R. W. Gerchberg, J. Mod. Opt. **49**, 1185 (2002).
[10] R. W. Gerchberg *et al.*, Optik (Stuttgart) **35**, 237 (1972).
[11] W. O. Saxton, *Computer Techniques for Image Processing in Electron Microscopy* (Academic Press, New York, 1978).
[12] J. R. Fienup, Appl. Opt. **21**, 2758 (1982).
[13] The routine employs the subspace trust region method from MATLAB©.
[14] M. Ibanescu *et al.*, Phys. Rev. E **67**, 046608 (2003).
[15] Y. Xu *et al.*, J. Lightwave Technol. **20**, 428 (2002).
[16] P. Yeh *et al.*, J. Opt. Soc. Am. **68**, 1196 (1978).
[17] B. Temelkuran *et al.*, Nature (London) **420**, 650 (2002).
[18] S. G. Johnson *et al.*, Opt. Express **9**, 748 (2001).
[19] K. S. Lee *et al.*, J. Opt. Soc. Am. A **18**, 1176 (2001).
[20] B. Z. Katsenelenbaum *et al.*, *Theory of Nonuniform Waveguides: The Cross-Section Method* (Institution of Electrical Engineers, London, 1998).